ている。染色体異常の誘発の軽減化にはDSBの修復効率の上昇が寄与する可能性が考えられ、すでに、この可能性を示唆する報告がなされている(8他)。私たちも、低線量の放射線照射による一連の変異誘発研究(9−12)に用いてきた、ヒトリンパ芽球細胞 TK6を利用して、放射線照射後に誘発される突然変異が軽減化される現象、適応応答の検出に成功した(13)。そこで、観察された変異誘発の軽減化にDSBの修復が影響を与えているかどうかに興味がもたれた。

本格的急照射はもとより、前照射によっても染色体DNAにDSBが生成されるので、これらの修復を測定するには両者を区別する必要がある。そこで、本格急照射の代わりに、制限酵素I-SceI発現ベクターの感染により、細胞内染色体の特定部位にDSBを生成させ、そのDSB修復効率を測定することにした。すなわち、変異誘発の軽減化が認められた適応応答誘導条件下で、DSB修復に及ぼす前照射の影響が認められるか否かの検証である。

幸いにも、I-SceI系によるDSB修復の測定が、低線量X線照射による適応応答反応や低線量・低線量率γ線による擬似適応応答反応の解明に貢献できる見通しが立ったので、以下に紹介する。

2．DSB修復を調べる系（I-SceI系）の構築

本間を中心にして私たちは、制限酵素I-SceI発現ベクターにより染色体のチミジンキナーゼ（*TK*）遺伝子座の特定部位（制限酵素I-SceI認識部位）にDSBを導入する系(14～16)を、ヒトリンパ芽球TK6細胞を用いて樹立した（図１ａ）。始めに、TK6細胞（*TK*+/−ヘテロ体）で機

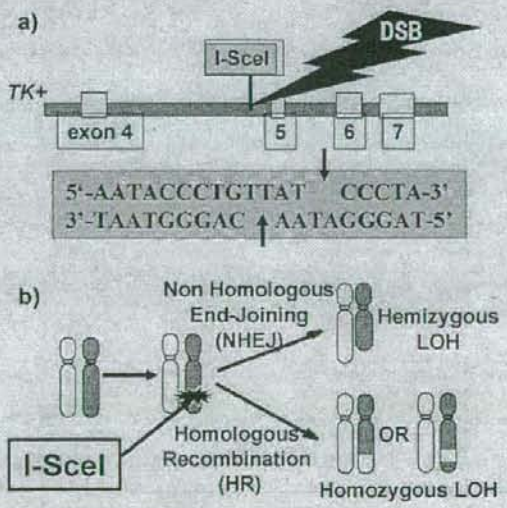

図１　制限酵素I-SceIの発現によるDSBの生成と修復の原理

ａ）TK6細胞のチミジンキナーゼ(*TK*)遺伝子座内の18塩基のI-SceI認識部位がDSBの標的となっている。

ｂ）ヘテロな*TK*遺伝子をもつTK6細胞では、DSB修復主要２経路であるNHEJとHRが働くと、それぞれHemizygous LOHとHomozygous LOHを誘発する。

能しているTK遺伝子座を遺伝子ターゲッティングベクターpTK4によってエキソン5の位置をneo耐性遺伝子で置き換えた。次に、I-SceI認識部位を導入するため、2番目の遺伝子ターゲッティングベクターpTK10（約6kbのオリジナルなTK遺伝子エクソン5，6，7領域とI-SceI認識部位をエクソン5の75bp上流にもつ）で先程壊した領域を置き換えた。このようにして新しく樹立された細胞をTSCE5細胞と名づけた（図2）。次に、TSCE5細胞の自然復帰変異体（*TK*−/−：TKコンパウンドヘテロ体、エキソン5の23番目のコドンにG→A変異）を取得することに成功し、TSCER2と名づけた（図2）。これらの細胞をI-SceIベクターpCBASceで感染後に、TSCE5細胞ではTFT耐性を指標にしてTK⁻ Forward変異を、TSCER2細胞ではHAT耐性を指標にしてTK⁺復帰変異の誘発頻度を測定することにより、DSBの修復効率を推測する系を構築した（図3）。DSBの修復には主に2つの経路、非相同末端結合（Non homologous end-joining: NHEJ）と相同組換え（Homologous recombination: HR）が知られている(17,18)が，NHEJによって生ずる欠失変異をForward Mutantとして，HRによって生ずる組換え変異体をRevertantとして検出し、DSB修復効率を測定する系である（図1b、3）。実際に、この系でDSB修復効率を測定すると、NHEJの方がHRよりもおよそ100倍も効率よくDSBを修復できることが明らかになった(14)。最近になって、I-SceI発現ベクターの高効率導入（100個の細胞のうち1個以上：従来の100倍）を可能にするエテクトロポレーションの条件を確立することができ、より高精度の実験を行っても同じ傾向を示した(15,16)。哺乳類細胞の電離放射線照射によって生ずるDSBがHRよりもNHEJによってより効率よく修復されるという従来の知見とも一致することから、放射線照射により生成されるDSBの修復モデルになりうるもの考えられる。しかしながら、この系ではG₂・S期の娘染色体交

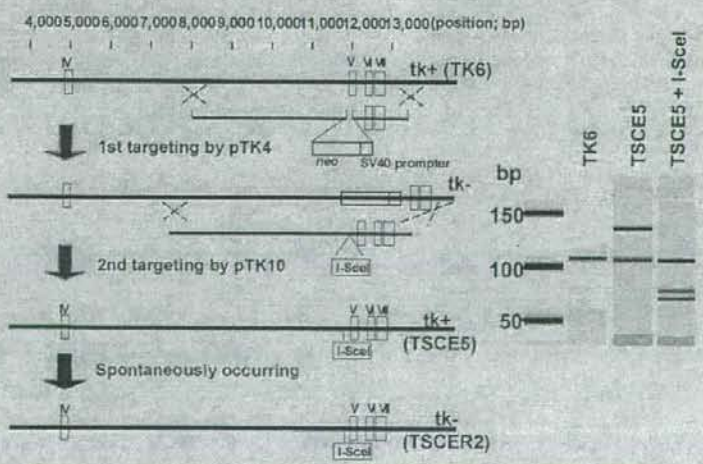

図2　制限酵素I-SceI認識部位をもつ細胞株の樹立
2回の遺伝子ターゲッティング法により薬剤マーカーなどを指標にしてTSCE5細胞を樹立し、次に、TSCE5細胞の自然復帰変異細胞（HAT耐性株）としてTSCER2細胞を分離した。

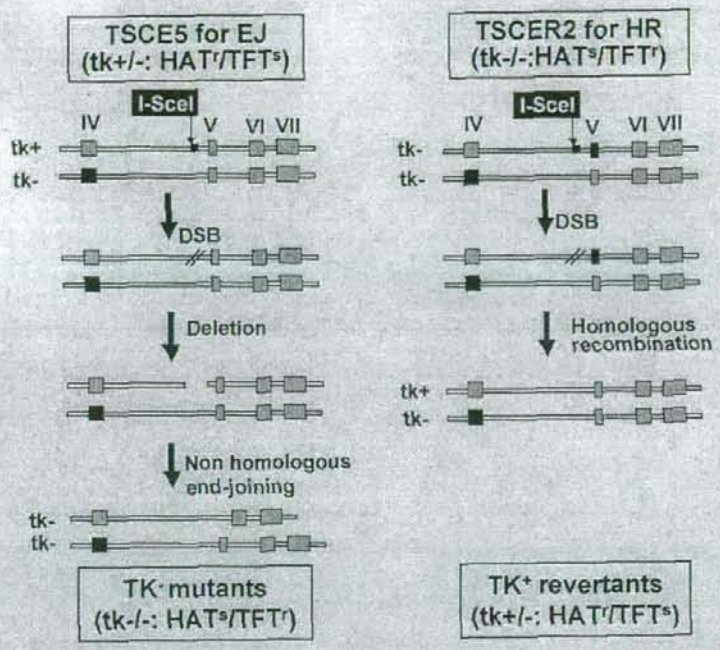

図3　DSB修復効率のLOH誘発頻度からの推測
樹立した細胞株によるDSB修復効率の測定原理を模式的に示した図で、NHEJはTSCE5細胞のTK(−)変異の誘発率から、HRはTSCER2細胞のTK(+)復帰の誘発率からDSB修復効率を測定する。

換におけるHRの寄与を考慮できない点などから、DSB修復におけるNHEJの寄与をHRの場合よりも相対的に過大評価している可能性は否定できない。

ここでは、DSB修復に及ぼす様々な因子の影響を調べるには、このI-SceI系が大変好都合であることを強調させていただきたい。その一例として、適応応答現象の推測に役だつことを以下に述べる。

3．I-SceI系によるDSB修復の測定

1）低線量X線照射による適応応答

TK6細胞に低線量のX線前照射を行うと、その後の本格X線照射によるTK突然変異の誘発が前照射なしの場合よりも低くなる、すなわち、変異の誘発が軽減化される現象を見つけた(13)。このことが、一連の適応応答研究のきっかけである。軽減化の最適条件を検討したところ、前照射の低線量は5cGy、本格的照射の線量は2Gy、前照射と本格照射のインターバルは6時間であった（図4a）。この条件下では、前照射は、本格照射によるTK突然変異誘発率を60%程度［$(18.3\pm4.3)\times10^{-6}\rightarrow(11.4\pm5.1)\times10^{-6}$; $P=0.020$］に低下させた。選択した変異細胞に対して、

ヘテロ接合性の喪失（Loss of Heterozygosity: LOH）を調べる解析(19)を試みたところ、DNA塩基損傷などが原因で起こる点突然変異型などの比較的小さな変異（非LOH型変異）はもとの25%程度（$7.1\times10^{-6}\rightarrow1.9\times10^{-6}$）まで大きく減少し、相同組換えによるホモ型LOHも、もとの60%程度まで低下（$5.1\times10^{-6}\rightarrow 3.1\times10^{-6}$）することが明らかになった（図4 b）。そこで、非LOH型変異のDNAシーケンスによる詳細解析や、遺伝子発現のウエスタンブロット解析やマイクロアレイ解析などで、得られた現象の解明を進めてきたが、紙面の都合上、省略する。ここでは、I-SceI系によるDSB修復の解析からの現象解明研究に的を絞って述べる。

上述の変異誘発を調べた「適応応答実験」（図4 a）における本格X線照射の処理の代わりに、細胞内で制限酵素I-SceIを発現させる上述の処理に行い、人為的染色体DNA2重鎖切断（DSB）を生成させ、その修復に及ぼす前照射（5cGy）の影響を検討した。得られた実験結果（投稿中）では、DSB修復への寄与がマイナーな経路、相同組換え経路によるDSB修復の効率は、前照射をすると、しない場合に比べて70%程度増加した（表1）。いっぽう、DSB修復に大きな寄与をしているメジャーな経路、非相同末端結合経路によるDSB修復の効率に対する前照射の影響は殆ど

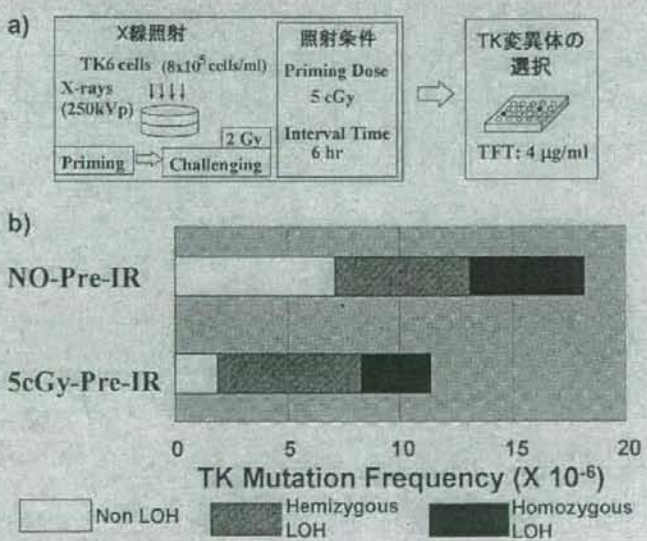

図4　ヤグルマギクの紫外線適応応答
左はヤグマギクの培養細胞にあらかじめUVBを照射した場合（実線）と照射しなかった場合（破線）で各波長での光吸収量を測定した。波形からフラボノイドであることが予測できる。特にUVB・UVCに吸収ピークをもち，UVからの影響を軽減する可能性が高いことが推測できる。中央はヤグマギクの培養細胞の生存率を測定した。あらかじめUVBで照射しておくと紫外線（UVC）に抵抗性になる。右はDNA損傷であるピリミジンダイマーを定量した。あらかじめUVBで照射しておくと、紫外線（UVC）によって生成されるDNA損傷であるピリミジンダイマー量が少なくなる。

表1　プレ・X線照射のDSB修復に及ぼす影響（モードA）

a) NHEJ の評価（TSCE5 細胞）

Exp.	Effect of IR* (Relative MF)
1	0.98
2	0.76
3	0.99
Average	0.91

*Relative MF は各実験の MF (X-rays+I-SceI) / MF (I-SceI) から計算(表 2 を参照)

b) HR の評価（TSCR2 細胞）

Exp.	Effect of IR* (Relative RF)
1	2.2
2	1.2
3	1.7
Average	1.7

*Relative RF は各実験の RF (X-rays+I-SceI) / RF (I-SceI) から計算(表 2 を参照)

表2　プレ・ガンマ線照射のDSB修復に及ぼす影響（モードA）

a) NHEJ による DSB 修復への寄与の相対評価（TSCE5 細胞）

Exp.	Mutant Frequency, MF (X 10^{-6})				Effect of IR* (Relative MF)
	Control	γ-rays	I-SceI	γ-rays + I-SceI	
1	3.5	6.1	8600	8500	0.99
2	1.8	3.2	2900	3200	1.1
Average	2.7	4.7	5800	5900	1.1

*Relative MF は各実験の MF (γ-rays+I-SceI) / MF (I-SceI) から計算

b) HR による DSB 修復への寄与 の相対評価 （TSCER2 細胞）

Exp.	Revertant Frequency, RF (X 10^{-6})				Effect of IR* (Relative RF)
	Control	γ-rays	I-SceI	γ-rays + I-SceI	
1	-	-	90	114	1.3
2	-	-	62	96	1.5
3	-	-	25	45	1.8
Average	-	-	59	85	1.5

*Relative RF は各実験の RF (γ-rays+I-SceI) / RF (I-SceI) から計算

表3　ポスト・ガンマ線照射のDSB修復に及ぼす影響（モードB）

a) NHEJ による DSB 修復への寄与の相対評価（TSCE5 細胞）

Exp.	Mutant Frequency, MF (X 10^{-6})				Effect of IR* (Relative MF)
	Control	γ-rays	I-SceI	γ-rays + I-SceI	
1	2.8	1.3	3400	4500	1.3
2	3.1	2.8	12000	17000	1.4
3	-	-	11000	11000	1.0
Average	3.0	2.1	8800	10800	1.2

*Relative MF は各実験の MF (γ-rays+I-SceI) / MF (I-SceI) から計算

b) HR による DSB 修復への寄与 の相対評価 （TSCER2 細胞）

Exp.	Revertant Frequency, RF (X 10^{-6})				Effect of IR* (Relative RF)
	Control	γ-rays	I-SceI	γ-rays + I-SceI	
1	-	-	82	160	2.0
2	-	-	160	270	1.7
3	-	-	110	190	1.7
Average	-	-	120	210	1.8

*Relative RF は各実験の RF (γ-rays+I-SceI) / RF (I-SceI) から計算

認められなかった。これらの結果は、本適応応答実験系で点突然変異など小さな変異の誘発が主に抑制され、ホモ型LOHの誘発も減少した遺伝解析結果と矛盾しない。なお、表1におけるNHEJおよびHRによるDSB修復への相対的寄与の求め方は、以下に述べる、低線量・低線量率γ線照射による同様の解析実験(16)の場合と全く同じである（表2，3を参照)。

2）低線量・低線量率γ線照射のDSB修復への影響

図5のような2条件で細胞を炭酸ガス培養器で細胞を培養しながらγ線を照射する装置（放射線医学総合研究所）を利用して、これらのγ線照射がI-SceI酵素により生成されるDSBの修復にどのような影響を及ぼすかを調べた(16)。図5aには実験条件Aが図5bには実験条件Bが模式的に示されている。条件Aは、上述の低線量X線照射による適応応答実験と類似しており、低線量X線が低線量・低線量率γ線に置き換わった実験であり、従来から提案されている適応実験の概念に基づいている。I-SceI発現ベクターは細胞に感染後、その発現が3日間程度持続することが確かめられているので、条件Bは、低線量・低線量率γ線で被ばく中にDSBが起きたときの細胞の応答を推測するための組み立てとみなせる。この条件を新しい概念の適応応答と呼ぶか否かは議論の分かれるところであろう。なお、条件Bは条件Aの場合に比べて、総線量で30%弱、線量率で10%くらいになっている。両条件による実験結果は、上述の低線量X線照射による適応応答条件下での結果と全く同様に、NHEJは影響を受けずに、HRは増強されるという傾向を示した

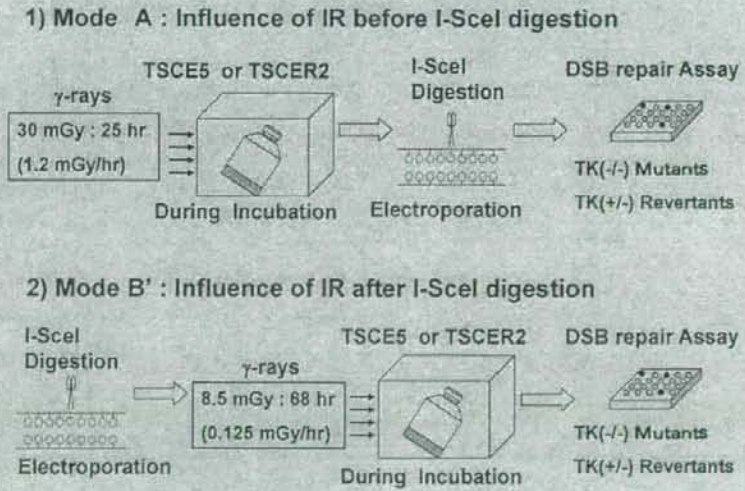

図5　低線量・低線量率ガンマ線照射によるDSB修復効率に及ぼす影響

1）Mode A：予めの低線量/低線量率γ線（1.2mGy/hr，30mGy：条件A）照射がDSB修復効率に及ぼす影響を調べる実験の手順

2）Mode B：DSB生成後のより低線量/低線量率γ線 照射(0.125mGy/hr，8.5mGy：条件B）によるDSB修復効率への影響を調べる実験の手順

(表2)。まとめると、以下のようになる。

① 予めの低線量/低線量率γ線（1.2mGy/hr，30mGy：条件A）照射によって、DSBのHR経路による修復効率が50％程度増加する。

② I-SceI発現ベクター感染後のより低線量/低線量率γ線 照射（0.125mGy/hr，8.5mGy：条件B）では、照射によってDSBのHR修復効率の増加の割合は80％程度増加する。

4．I-SceI系の応用と考察

1）応用

このI-SceI系は、宇宙放射線、低重力などの宇宙環境因子の生物影響を明らかにする研究にも有望と考えられる。2008年11月にスペースシャトルで凍結状態のTK6細胞を打ち上げ、ISSのきぼう棟でおよそ3ヶ月間凍結保存し、地上に回収してから、I-SceI制限酵素の発現によって生成させたDSBの修復を検討する計画を進めている。果たして、宙環境下に細胞を長期凍結保存した場合に、宇宙放射線を低線量率で被ばくされ続けた効果が積算されて、地上の適応応答実験の前照射の線量に到達できるかどうかぎりぎりであるが、地上回収後の適応応答として被ばくの影響を検出することにチャレンジする。なお、この宇宙実験のシミュレーション実験として、理研リングサイクロトロンによって加速した炭素イオン(135MeV/u)を凍結TK6細胞に50mGy照射して、その後1，2カ月、−80℃に凍結保存した後に、このI-SceI系によるDSB修復の測定を行ったところ、上述の適応応答実験の場合と同様に、HRによるDSB修復の効率は、炭素イオンを照射しなかった場合よりも高くなる傾向が得られている（未発表）。

いっぽう、生体内に微量元素としていくつかの金属元素が知られている。その中でも、亜鉛は鉄に続いて多く存在し、生体に投与されると、酸化的ストレスを誘導し、DNA損傷、タンパク質（熱ショックタンパク質やメタロチオネイン）の合成を誘導する(20)とともに、発現されたメタロチオネインによってストレスが軽減されると考えられている(21)。実際にマウスやウサギを用いた実験系で、亜鉛の事前投与により、放射線照射後の生存率の向上やリンパ球の染色体損傷が軽減されることが報告されている(22,23)。この現象は、「亜鉛による細胞機能の調節とがん」というタイトルの渡辺らによる本誌の総説(24)の中でも紹介されているが、やはり、適応応答として捉えることができるものと思われる。果たして、ここで紹介したI-SceI系を利用した細胞レベルの実験でも再現できるのであろうか。早い機会に、この種の実験にも着手したい。

2）考察

ここで紹介した、制限酵素I-SceIによる染色体の特定部位切断を導入する系について以下の問題点があげられる。

① I-SceIにより生成されるDSBが電離放射線によって生成されるDSBとは全く同じ切断末端をもっていない

② NHEJによる、DSBの正確な再結合およびエクソン領域に限定された小さな欠失変異を伴う修復はこの系では検出されない。

③ 比較的高い線量により複数のDSBが近接して生じた場合の推測はできない。

これらの問題点が、本I-SceI系による適応応答の測定でNHEJによるDSB修復の効率の上昇が観測されなかった原因になったのではないかと推測される。今後、NHEJによるDSB修復の効率が適応応答で本当に上昇しないのかという問題は別の系で確かめなければならない。さらに、HR反応で重要な役割を果たしているRad51の寄与(25他)を含めて、ここで観察されたHR活性上昇の分子メカニズムを追及しなければならない。

しかしながら、放射線の直接的作用ではなく間接作用を推測するために、このI-SceI系によるDSB修復効率の測定は大変有用と考えられる。言うまでも無く、間接効果の中で適応応答は最も重要な現象のひとつである。

5．終りに（謝辞）

本誌に執筆の機会を与えていただいた、奈良県立医科大学の大西武雄教授を始めとして、本研究を支えてくれた関係各位に深く感謝の意を表したい。放射線医学総合研究所の鈴木雅夫博士の低線量・低線量率ガンマ線照射に関するご指導とご協力がなければ、本研究は成立していない。ここでは、新原子力基盤クロスオーバー研究「低線量放射線に特有な生体反応の多面的解析」の分担課題「適応応答の染色体レベルでの検証と分子レベルでの解析」を進める過程で得られた研究成果を中心に紹介させていただいたが、国際宇宙ステーションを利用する宇宙実験プロジェクトの地上準備実験研究による成果なども含まれている。

参考文献

1. Wolf, S. Aspects of the adaptive response to very low doses of radiation and other agents. Mutat. Res., 358: 135-142, 1996.
2. Wolf, S. The adaptive response in radiobiology: Evolving insights and implications. Environ. Health Pesrpect., 106: 277-283, 1998.
3. 松本英樹、林幸子、金朝暉、畑下昌範、加納永一、放射線適応応答とバイスタンダー効果、放射線生物研究、37: 420-430, 2002.
4. 大西武雄、高橋昭久、放射線適応応答のしくみの再考、放射線生物研究、43: 91-99, 2008.
5. Olivieri, G., Bodycote, Y., and Wolf, S. Adaptive response of human lymphocytes to low concentrations of radioactive thymidine. Science 223: 594-597, 1984.
6. Ikushima, T. Chromosomal response to ionizing radiation reminiscent of an adaptive response in cultured chinese hamster cells. Mutat. Res., 180: 215-221, 1987.
7. Rigaud, O., Papadopoulo,D., and Moustacchi, E. Decreased deletion mutation in radioadapted human lymphoblast. Radiat. Res., 133: 94-101, 1993.
8. Ikushima, T., Aritomi, H., and Morisita, J. Radioadaptive response: efficient repair of radiation-induced DNA damage in adapted cells. Mutat. Res., 358: 93-198, 1996.
9. Morimoto, S., Kato, T., Honma, M., Hayashi, M., Hanaoka, F., and Yatagai, F.: Detection of genetic alterations induced by low-dose X-rays: Analysis of loss of heterozygosity for *TK* mutation in human lymphoblastoid cells., Radiat. Res., 157: 533-538, 2002.
10. Morimoto, S., Honma, M., and Yatagai, F.: Sensitive detection of LOH events in a human cell line after C-ion beam exposure, J. Radiat. Res., 43 Suppl.: 163-167, 2002.
11. Umebayashi, Y., Honma, M., Abe, T., Ryuto, H., Suzuki, H., Shimazu, T., Ishioka, N., Iwaki, M., and Yatagai, F. Mutation induction after low-dose carbon ion beam irradiation. Biol. Sci. Space. 19: 237-241, 2005.
12. Umebayashi, Y., Honma, M., Suzuki, M., Suzuki, H., Shimazu, T., Ishioka, N., Iwaki, M., and Yatagai, F. Mutation induction in cultured human cells after low-dose and low-dose-rate γ-ray irradiation: Detection by LOH analysis. J. Radiat. Res., 48: 7-11, 2007.
13. Yatagai, F., Umebayashi, Y., Honma, M., Sugasawa, K., Takayama, Y., and Hanaoka, F. Mutagenic radioadaptation in a human lymphoblastoid cell line. Mutat. Res., 638: 48-55, 2008.
14. Honma, M., Izumi, M., Sakuraba, M., Tadokoro, S., Sakamoto, H., Wang, W., Yatagai, F., and Hayashi, M. Deletion, rearrangement, and gene conversion; Genetic consequences of

chromosomal double-strand breaks in human cells. Environ. Mol. Mutagen. 42: 288-298, 2003.

15. Honma, M., Sakuraba, M., Koizumi, T., Takashima, T., Sakamoto, H., and Hayashi, M. Non-homologous end-joining for repairing I-SceI induced DNA double strand breaks in human cells. DNA Repair 6: 781-788, 2007.
16. Yatagai, F., Suzuki, M., Ishioka, N., Ohmori, H., and Honma, M. Repair of I-SceI induced DSB at a specific site of chromosome in human cells: Influence of low-dose, low-dose-rate gamma-rays. Radiat. Environ. Biophys. 47: 439-444, 2008.
17. Jackson, S.P. Sensing and repairing DNA double-strand breaks. Carcinogenesis 23: 687-696, 2002.
18. Valerie, K., and Povirk, L.F. Regulation and Mechanisms of mammalian double-strand break repair. Oncogene 22: 5792-5812, 2003.
19. Yatagai, F., Morimoto, S., Kato, T., and Honma, M. Further characterization of loss of heterozygosity enhanced by p53 abrogation in human lymphoblastoid TK6 cells: disappearanace of endopoint hotspots. Mutat. Res., 560: 133-145, 2004.
20. Stohs, S.J., and Baguchi, D. Oxidative mechanisms in the toxicity of metal ions. Free Radic. Biol. Med., 2: 321-336, 1995.
21. Park, J.D., Liu, Y., and Klassen, C.D. Protective effect of metallothionein against the toxicity of cadmium and other metals (I). Toxicology, 163: 93-100, 2001.
22. Matsubara, J., Tajima, Y., and Karasawa, M. Promotion of radioresistance by metallothionein induction prior to irradiation. Environ. Res., 43: 66-74, 1987.
23. Cai, L., and Cherian, M.G. Adaptive response to ionizing radiation-induced chromosome aberrations in rabbit lymphocytes: Effect of pre-exposure to Zinc, and copper salts. Mutat. Res., 369: 233-241, 1996.
24. 渡辺健一、今岡達彦、柿沼志津子、西村まゆみ、島田義也、亜鉛による細胞機能の調節とがん、放射線生物研究 39(1), 48-56, 2004.
25. Li, X., and Heyer, W.-D. Homologous recopmbination in DNA repair and DNA damage tolerance. Cell Res., 18: 99-113, 2008.

Journal of Neuroscience Research 86:929–936 (2008)

Up-Regulated Neuronal COX-2 Expression After Cortical Spreading Depression Is Involved in Non-REM Sleep Induction in Rats

Yilong Cui,[1,2,3] Yosky Kataoka,[1,3,4]* Takashi Inui,[5] Takatoshi Mochizuki,[5] Hirotaka Onoe,[1,3] Kiyoshi Matsumura,[3] Yoshihiro Urade,[5] Hisao Yamada,[2] and Yasuyoshi Watanabe[1,3,4]

[1]Molecular Imaging Research Program, Institute of Physical and Chemical Research (RIKEN), Kobe, Hyogo, Japan
[2]Department of Anatomy and Cell Science, Kansai Medical University, Moriguchi, Osaka, Japan
[3]Department of Neuroscience, Osaka Bioscience Institute, Suita, Osaka, Japan
[4]Department of Physiology, Osaka City University Graduate School of Medicine, Abeno-ku, Osaka, Japan
[5]Department of Molecular Behavioral Biology, Osaka Bioscience Institute, Suita, Osaka, Japan

Cortical spreading depression is an excitatory wave of depolarization spreading throughout cerebral cortex at a rate of 2–5 mm/min and has been implicated in various neurological disorders, such as epilepsy, migraine aura, and trauma. Although sleepiness or sleep is often induced by these neurological disorders, the cellular and molecular mechanism has remained unclear. To investigate whether and how the sleep-wake behavior is altered by such aberrant brain activity, we induced cortical spreading depression in freely moving rats, monitoring REM and non-REM (NREM) sleep and sleep-associated changes in cyclooxygenase (COX)-2 and prostaglandins (PGs). In such a model for aberrant neuronal excitation in the cerebral cortex, the amount of NREM sleep, but not of REM sleep, increased subsequently for several hours, with an up-regulated expression of COX-2 in cortical neurons and considerable production of PGs. A specific inhibitor of COX-2 completely arrested the increase in NREM sleep. These results indicate that up-regulated neuronal COX-2 would be involved in aberrant brain excitation-induced NREM sleep via production of PGs.

Key words: aberrant excitation; prostaglandin; spreading depression; sleep; cyclooxygenase-2

Cortical spreading depression (SD) was described first by Leao (1944), and characterized by a transient negative shift of direct current (DC) potential (Nedergaard and Hansen, 1988) and temporal elevation of cerebral blood flow (CBF; Fabricius et al., 1995; Shimizu et al., 2000). It is due to a self-propagating front of depolarization that begins in the neuronal and/or glial cells of local areas of the brain and subsequently spreads in all directions at a rate of approximately 2–5 mm/min (Leao, 1944; Shinohara et al., 1979; Hansen and Zeuthen, 1981; Lauritzen et al., 1982). SD has been implicated in the pathophysiological states of various neurological disorders, such as epilepsy, migraine aura, and trauma (Gorji, 2001), which are accompanied by an aberrant neuronal excitation in the brain. Although it is well known empirically that sleepiness or sleep is often induced by these neurological disorders (Sand, 1991; Donnet and Bartolomei, 1997; Foldvary, 2002), the cellular and molecular mechanism of the sleep induction has remained unclear.

Cyclooxygenase (COX)-2 is now known to be constitutively expressed in the central nervous system in restricted neuronal populations, including cerebral cortical and hippocampal neurons. Neuronal COX-2 expression is regulated by neural activity, such as synaptic activity or membrane depolarization accompanied by Ca^{2+} loading in cells (Koistinaho and Chan, 2000; Yermakova and O'Banion, 2000), and its expression is dramatically increased in a variety of neurological disorders, such as epilepsy, migraine aura, and trauma (Yamagata et al., 1993; Nogawa et al., 1997; Strauss et al., 2000). COX-2 is a rate-limiting enzyme of the arachidonic acid cascade and triggers production of prostaglandins (PG) and other related substances. PGs play important and diverse roles

Contract grant sponsor: Ministry of Education, Culture, Sports, Science and Technology of the Japanese Government (to Y.K.); Contract grant sponsor: Japan Society for the Promotion of Science; Contract grant number: 16700291 (to Y.C.).

*Correspondence to: Yosky Kataoka, Department of Physiology, Osaka City University Graduate School of Medicine, 1-4-3 Asahimachi, Abeno-ku, Osaka 545-8585, Japan. E-mail: kataokay@med.osaka-cu.ac.jp

Received 19 June 2007; Revised 24 July 2007; Accepted 26 July 2007

Published online 10 October 2007 in Wiley InterScience (www.interscience.wiley.com). DOI: 10.1002/jnr.21531

in the central nervous system. A variety of central actions have been demonstrated, such as regulation of sleep-wake cycle (Hayaishi, 1988; Hayaishi and Urade, 2002), body temperature (Ueno et al., 1982), and luteinizing hormone-releasing hormone (LHRH) secretion (Ojeda et al., 1982) and potentiation of the action of excitatory amino acids on Purkinje cell dendrites (Kimura et al., 1985). These observations raise the possibility that up-regulated neuronal COX-2 after aberrant neuronal excitation in these neurological disorders is involved in sleep induction via triggering production of PGs; however, no literature has clarified this.

To investigate whether and how the sleep-wake behavior is altered by aberrant brain activity, we induced cortical SD in freely moving rats and investigated the functional role of neuronal COX-2 in sleep induction. SD can be remotely induced in the animals under the freely moving condition, by photodynamic oxidation of a local region of the cerebral cortex using a glass fiber (Kataoka et al., 2000; Cui et al., 2003). Here we provide a new line of evidence that neuronal COX-2 is involved in signal regulation of non-REM (NREM) sleep induction after aberrant neuronal excitation in the cerebral cortex.

MATERIALS AND METHODS

All experimental protocols were approved by the Ethics Committee on Animal Care and Use of Kansai Medical University and were performed in accordance with the *Principles of laboratory animal care* (NIH publication No.85-23, revised 1985).

Animal Preparation for Generation of Spreading Depression in Freely Moving Rats

Cortical SD was generated in freely moving male Sprague-Dawley rats (weighing about 300 g; SLC, Hamamatsu, Japan) using the photodynamic tissue oxidation (PDTO) technique (Kataoka et al., 2000; Cui et al., 2003). The animals were housed before experimentation in a soundproof chamber (ambient temperature 25°C, relative humidity 60%). The chamber was maintained on a 12:12-hr light:dark cycle (lights on at 8 AM), and standard laboratory rat chow and water were supplied ad libitum. The animals were anesthetized with 4.0% halothane, and anesthesia was maintained with 1.0% halothane in air. The head of each animal was fixed in a stereotaxic apparatus (type 1430; David Kopf, Tujunga, CA). A small burr hole for injection of rose Bengal was drilled in the skull at the frontal cortex (2.0–3.0 mm anterior and 2.0–3.0 mm lateral to the bregma). Then, rose Bengal (3 mM, 1.6 μl) was injected through a glass micropipette (internal diameter of the tip 50 μm) into the frontal cortex (0.5–2.0 mm ventral to the cortical surface) taking 40 min in a dark room. A short plastic cannula for guiding the tip of a glass fiber on the rose Bengal-injected area was fixed on the burr hole by instant adhesive. A plug was kept in the cannula to prevent photoactivation of rose Bengal by room light before the experiments.

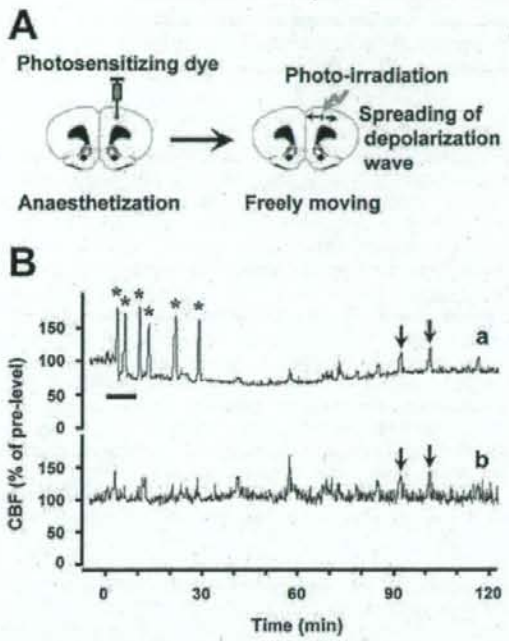

Fig. 1. Cortical spreading depression (SD) in freely moving rats. **A:** The photodynamic tissue oxidation (PDTO) procedure for inducing SD in the cortical hemisphere of a freely moving rat. **B:** Cerebral blood flow (CBF) changes in a freely moving animal. Two laser Doppler flowmeter (LDF) probes were placed [one on the parietal cortex of the PDTO-treated brain hemisphere (a) and one on the opposite side (b)]. While the animal was freely moving, the rose Bengal-injected site in the frontal cortex was photoirradiated (540–580 nm and 380 mW/cm^2) via a glass fiber. Bar in the upper panel indicates photoirradiation lasting 10 min. Asterisks indicate SD-associated hyperperfusion events. Note that some irregular fluctuations of the CBF, indicated by an arrow, were concomitantly observed in both hemispheres.

Cerebral Blood Flow Recording

Five of the rose Bengal-injected rats were used for recording cerebral blood flow (CBF). The CBF was detected with laser Doppler flowmetry (LDF; type FLO-N1; Omegawave, Tokyo, Japan). Immediately after the rose Bengal injection, one LDF probe (0.2 mm diameter) was inserted into each of two small burr holes (previously drilled in the skull, 7 mm posterior to the dye-injected area and on the hemispherically opposite side). The plastic cannula and LDF probes were rigidly fixed to the skull with dental acrylic cement, and two screws anchored them to the skull. The rats were returned to their cages for 3–4 hr and allowed free movement. The plug in the plastic cannula was replaced with a glass fiber (1 mm diameter), and the rose Bengal-injected area was photoirradiated (metal halide lamp, 540–580 nm, and 380 mW/cm^2) via the glass fiber (see Fig. 1A). The laser Doppler flowmeter

does not measure actual perfusion units, so percentage of change in CBF was determined (the data were normalized to 5 min of pre-PDTO values).

Sleep Monitoring

The vigilance stages were monitored in 15 rose Bengal-injected and 6 vehicle-injected rats using EEG and electromyography (EMG). Because SD reduces cortical EEG amplitude (Leao, 1944) in the treated hemisphere by causing a transient membrane depolarization in the neurons, we recorded EEG signals from the opposite hemisphere. Immediately after the rose Bengal injection, three Teflon-coated stainless-steel wire electrodes bared at the tip were chronically implanted into the parietal cortex of the hemisphere opposite to the dye-injected cortex for EEG recordings. A stainless-steel screw attached to the frontal region of the skull served as the ground electrode. Two stainless-steel wire electrodes were inserted into the neck muscles for EMG recordings. The plastic cannula and electrodes were rigidly fixed to the skull with dental acrylic cement, and three screws anchored them to the skull.

After housing each animal in the experimental chamber for 3 days, the plug in the plastic cannula was replaced with a glass fiber (1 mm diameter), and the 24-hr polygraphic recordings of EEG and EMG were started at 2 PM. The rose Bengal-injected area was photoirradiated at 8 PM according to the same protocol used for generation of SD described above. At the end of the recording time, animals were perfused with 4% formaldehyde buffered with 0.1 M phosphate-buffered saline (PBS; pH 7.4) under deep anesthesia with diethyl ether. Then, a histological study was performed to check the position of EEG electrodes in the cerebral cortex.

The EEG/EMG signals were amplified, filtered (EEG 0.5–20 Hz, EMG 20–200 Hz), and recorded with a sampling rate of 128 Hz. The data were analyzed using an animal sleep analysis software package (SleepSign; Kissei Comtec, Matsumoto, Japan); the behavioral states of the animals were automatically classified into one of three stages (i.e., wakefulness, NREM, or REM sleep) every 4 sec, according to the standard criteria (Tobler et al., 1997; Gerashchenko et al., 2000; Huang et al., 2001). The automatically defined stages were verified by researchers.

PG Enzyme Immunoassay

Fifteen male Sprague Dawley rats were used for PG enzyme immunoassay. At 2 hr after onset of SD (induced by photooxidation for 30 min), rats were killed by an overdose of diethyl ether anesthesia. The heads were immediately frozen in liquid nitrogen. The whole brain was rapidly removed, weighed, and then homogenized in ethanol (pH 2.0) containing 0.02% HCl. The material was centrifuged at 500*g* for 20 min. ^{3}H-labeled PGD_2, PGE_2, and $PGF_{2\alpha}$ (60 Bq for each assay; New England Nuclear, Boston, MA) were added as tracers for estimating recovery to the supernatant. The PGs were extracted with ethyl acetate, which was evaporated under nitrogen, and then the samples were separated by HPLC as described previously (Pandey et al., 1995). The quantification of PGs was performed with enzyme immunoassay (EIA) using their EIA kits (Cayman Chemical, Ann Arbor, MI).

Immunohistochemistry

Localizations of COX-2 and lipocalin-type PGD synthase (L-PGDS) in the brain were immunohistochemically examined in five other rats. Two hours after onset of SD, each rat (under deep anaesthesia with diethyl ether) was perfused with 4% formaldehyde buffered with 0.1 M phosphate-buffered saline (PBS; pH 7.4). The brain was removed and further fixed in the same fixative for 24 hr at 4°C. We prepared coronal brain sections (30 μm thickness) using a cryostat and performed immunohistochemical studies. To immunostain COX-2, rabbit polyclonal antibody recognizing rat COX-2 (1:2,000; Cayman Chemical) was used. The bound antibodies were visualized by the avidin-biotin complex method (Vectastain ABC kit; Vector, Burlingame, CA). Double immunofluorescence staining of COX-2 and L-PGDS was carried out by a series of immunoreactions, first with rabbit polyclonal antibody recognizing rat L-PGDS (1:200), which was visualized by Cy2-conjugated secondary antibody (Jackson Immunoresearch, West Grove, PA) and then with rabbit polyclonal antibody recognizing rat COX-2, which was visualized by Cy5-conjugated secondary antibody (Jackson Immunoresearch). A confocal laser microscope (Zeiss LSM 510; Carl Zeiss, Oberkochen, Germany) was used for observation.

RESULTS

Spreading Depression in Freely Moving Rats

CBF was monitored after surgery at a site 7 mm posterior to the dye-injected area and at the corresponding site in the opposite hemisphere. After recovery from anesthesia, some irregular fluctuations of CBF were concomitantly recorded from both hemispheres (Fig. 1B). Such transient CBF changes are thought to reflect changes in local brain activities in freely moving animals. After placing each animal in the experimental chamber for 3–4 hr, the rose Bengal-injected area was photooxidized for 10 min. Beginning several minutes after the onset of photooxidation, changes in CBF [with amplitudes that were 71.7 ± 4.1% (mean ± SEM, n = 30 deflections in 5 animals) of that before photooxidation] were observed for approximately 1 hr in the photooxidized hemisphere but not in the opposite hemisphere, as is characteristic of SD (Cui et al., 2003). Such transient CBF changes are well known to be synchronously accompanied by the transient negative shifts of DC potential, as described in our previous report (Cui et al., 2003) and in other studies (Back et al., 1994; Gold et al., 1998). The small spontaneous fluctuations of CBF disappeared during the PDTO-induced SD in the photooxidized hemisphere. During the photooxidation and SD, the animals showed hypoactivity but not show hemiparalysis nor convulsion.

Increase in NREM Sleep Induced by Cortical SD

Sleep-wake behavioral states in freely moving rats, i.e., experimental (photoirradiated following rose Bengal

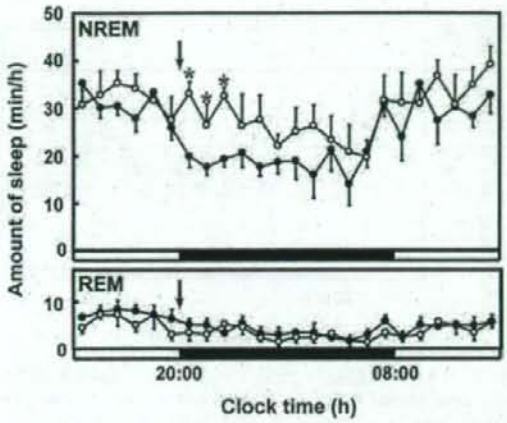

Fig. 2. Cortical spreading depression (SD)-induced NREM and REM sleep. Hourly changes of amounts of NREM sleep (NREM) and REM sleep (REM) were plotted for 24 hr (starting at 2 PM) in SD-induced (open circles, n = 5) and sham-operated (vehicle-injected) animals (solid circles, n = 6). Arrows indicate the 10-min photoirradiation period. *$P < 0.05$, two-way ANOVA, Scheffe's multiple-comparison procedure.

injection; n = 5 animals) and sham-operated (photoirradiated following vehicle injection; n = 6 animals), were evaluated on the basis of EEG and EMG criteria. The sham-operated animals exhibited a normal circadian reduction in the amount of NREM sleep during the dark period; the amount of NREM sleep decreased to approximately 18 min/hr (8 PM – 8 AM, dark) from 30 min/hr (8 AM – 8 PM, light). However, the amount of NREM sleep in the experimental relative to that in the sham-operated rats significantly increased for 3 hr following SD induction ($P < 0.05$, two-way ANOVA, Scheffe's multiple-comparison procedure; Fig. 2A). No significant differences in amount of REM sleep were noted between the experimental and sham-operated animals following SD induction ($P < 0.05$, two-way ANOVA, Scheffe's multiple-comparison procedure).

Neuronal COX-2 Expression and Production of PGs by Cortical SD

The COX-2 immunoreactivity was dramatically increased in neurons of layers II and III, with moderate expression in all the other cortical layers in the SD-induced cortical hemisphere (Fig. 3). Small numbers of COX-2-immunopositive neurons were scattered throughout the contralateral hemisphere and on both sides of the cerebral cortex of the untreated animals, indicating moderate constitutive expression of the enzyme in cortical neurons. Enzyme immunoassay on whole brain showed that the amounts of PGD_2, PGE_2, and $PGF_{2\alpha}$ in nontreated animals (n = 5 animals) were

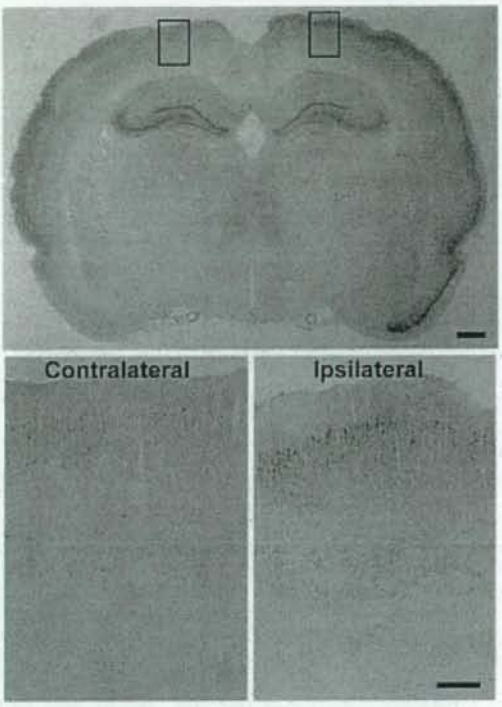

Fig. 3. Cortical spreading depression (SD) induced COX-2 expression in cortical neurons. Upper panel: Coronal view of the midcortex (a coronal section at 5 mm posterior to photooxidized area). Marked COX-2 immunoreactivity in cortical neurons of the hemisphere (the right side) 2 hr after onset of SD. Lower panel: Magnified views of areas indicated by the left (contralateral) and the right (ipsilateral) rectangles in upper panel. Scale bars = 1 mm in upper panel; 200 μm in lower panels.

281.7 ± 45.0, 92.7 ± 51.2, and 112.9 ± 4.1 pg/brain, respectively. The amounts of PGD_2, PGE_2, and $PGF_{2\alpha}$ were greatly increased (10- to 20-fold) 2 hr after onset of SD induction (n = 5 animals; Fig. 4). Rose Bengal without photoirradiation did not affect the level of PGs (n = 5 animals).

Selective COX-2 Inhibitor Completely Arrested the Neural Activity-Dependent NREM Sleep

To verify that neuronal COX-2 up-regulated by SD is involved in such NREM sleep induction, NS-398, a selective COX-2 inhibitor, was used to suppress COX-2 activity. One hour before photooxidation for induction of SD, NS-398 (5 mg/kg, n = 5 animals) or vehicle (n = 5 animals) was intraperitoneally injected. In animals pretreated with vehicle, the amount of NREM

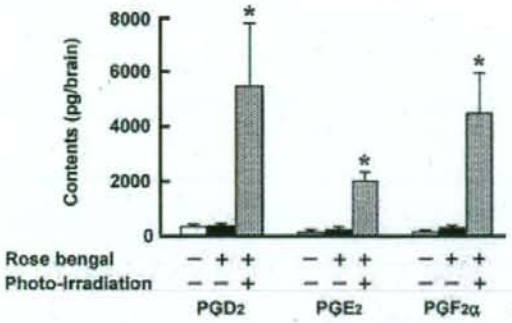

Fig. 4. Increased contents of PGD_2, PGE_2, and $PGF_{2\alpha}$ only in the cortical spreading depression (SD)-induced brain 2 hr after onset of SD. $*P < 0.05$, two-tailed unpaired *t*-test.

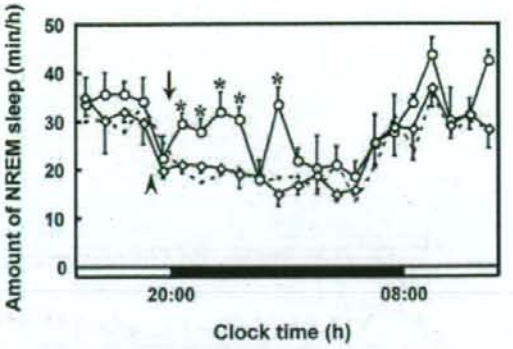

Fig. 5. NS-398, a selective COX-2 inhibitor, eliminated the cortical spreading depression (SD)-induced increment in NREM sleep. Hourly changes of amount of NREM sleep in animals pretreated with NS-398 (diamonds, n = 5) or pretreated with the vehicle (circles, n = 5). Arrowhead indicates the time of intraperitoneal injection of NS-398 or the vehicle; arrow indicates the time of SD induction in both animal groups; dashed line indicates amount of NREM sleep in the sham-operated animals that did not undergo SD induction. $*P < 0.05$, two-way ANOVA, Scheffe's multiple-comparison procedure.

sleep was significantly increased for 5 or 6 hr after photooxidation for 30 min ($P < 0.05$, two-way ANOVA, Scheffe's multiple-comparison procedure), which was longer than the photooxidation period (10 min) used to induce NREM sleep (3 hr increase; Fig. 5). On the other hand, in the animals pretreated with NS-398, the increment of NREM sleep after SD induction was completely abrogated (Fig. 5). NS-398 itself affected neither the number of induced SD nor the behavioral states of the animals (data not shown). These results indicate that the neuronal COX-2 regulates NREM sleep stemming from aberrant brain excitation but not sleep based on circadian rhythms.

DISCUSSION

In the present study, we first demonstrated that dramatically up-regulated neuronal COX-2 expression in the cerebral cortex after aberrant brain activity is involved in the induction of NREM sleep via triggering the production of PGs. We show here that 1) COX-2 immunoreactivity was dramatically increased only in neurons of the cerebral cortex that underwent SD; 2) the amount of NREM sleep but not of REM sleep increased in those animals and the increase lasted for several hours; 3) the contents of PGs were significantly increased in brain tissue; and 4) a selective COX-2 inhibitor, NS-398, prevented the NREM sleep increase.

COX-2 was initially characterized as an inducible enzyme that is expressed in response to inflammatory stimuli, cytokines, and mitogens in nonneuronal tissues (Yermakova and O'Banion, 2000; Schwab and Schluesener, 2003). In the central nervous system, COX-2 is now known to be constitutively expressed in restricted population of neurons, including cerebral cortex and hippocampus, and its expression is up-regulated by neural activity such as synaptic activity or membrane depolarization accompanied by Ca^{2+} loading in cells (Koistinaho and Chan, 2000; Yermakova and O'Banion, 2000). Neuronal COX-2 expression was dramatically increased in variety of neurological disorders such as epilepsy, migraine and trauma, which are accompanied by aberrant brain excitation (Yamagata et al., 1993; Nogawa et al., 1997; Strauss et al., 2000). Previously, up-regulation of neuronal COX-2 expression in the brain was also observed after SD (Caggiano et al., 1996; Miettinen et al., 1997). We found here that, consistently with these reports, neuronal COX-2 expression was dramatically increased in cerebral hemisphere following SD.

COX-2 is a rate-limiting enzyme of the arachidonic acid cascade responsible for the production of PGs. To investigate the possible pathway of PGs production catalyzed by neuronal COX-2, we also examined one kind of PG synthase, L-PGDS. L-PGDS immunoreactivity is widely distributed in the leptomeninges, choroid plexuses, and parenchymal oligodendrocytes, as previously reported (Beuckmann et al., 2000). Double-immunostaining study showed that many L-PGDS-immunopositive oligodendrocytes abut COX-2-immunopositive neurons, especially in cortical layers IV–VI in the SD-induced cerebral cortex (Fig. 6A). L-PGDS immunoreactivity, however, was not different between hemispheres 2 hr after onset of SD, indicating that expression of L-PGDS was not affected by SD (Fig. 6B). L-PGDS (a member of the lipocalin superfamily; Nagata et al., 1991) is secreted by oligodendrocytes and leptomeningeal cells into the extracellular space (Beuckmann et al., 2000). In addition, Yamagata et al. (1993) hypothesized that PGH_2 is highly lipid soluble and could

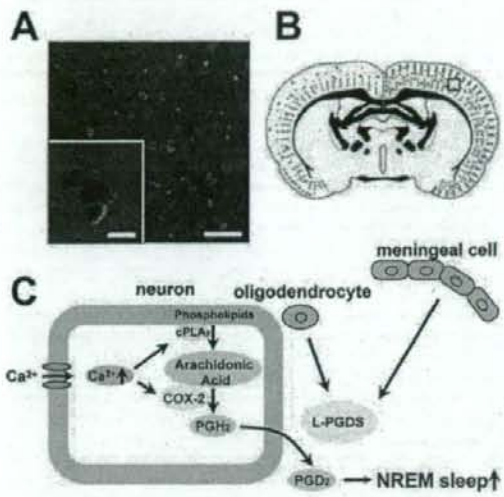

Fig. 6. Hypothetical role of the arachidonic acid cascade in increasing the amount of NREM sleep following excitation of cortical neurons. **A:** Confocal laser microscope images of immunohistochemically demonstrated COX-2 (red) and lipocalin-type prostaglandin D synthase (L-PGDS; green) in the area indicated by a rectangle in B. The **inset** clearly shows an L-PGDS-immunopositive cell abutting on a COX-2-immunopositive neuron. **B:** Drawing showing the localizations of COX-2 (red) and L-PGDS (green) 2 hr after onset of SD (the SD-induced side, right). **C:** Schema of the hypothetical mechanism of neuronal COX-2-induced NREM sleep following cortical neural activity. Scale bars = 50 μm in A; 10 μm in inset.

diffuse to the extracellular space or adjacent cells. These observations indicate that secreted L-PGDS from the leptomeninges or oligodendrocytes can convert PGH_2 produced by neuronal COX-2 into PGD_2 in the parenchymal extracellular matrix. Thus, induction of neuronal COX-2 by SD contributes at the very least to the rise in PGD_2.

PGs in the brain are known to possess sleep-promoting effects. Hayaishi and his coworkers demonstrated that content of PGD_2 in the cerebrospinal fluid of rats exhibited a circadian variation (Pandey et al., 1995) and that infusion of PGD_2 into the third ventricle or the subarachnoid space in the rostral basal forebrain induced NREM sleep in rats (Matsumura et al., 1994). After SD, PGH_2 produced by neuronal COX-2 likely increased the PGD_2 concentration in the cerebrospinal fluid and activated the sleep-promoting mechanism, as hypothesized by Hayaishi and colleagues (Fig. 6C; Hayaishi, 1988; Hayaishi and Urade, 2002). PGE_2 and $PGF_{2\alpha}$ were also reported to promote NREM sleep in rats when they were infused into the subarachnoid space in the rostral basal forebrain (Ram et al., 1997). Indeed, it has been reported that the amount of PGs dramatically increases (Forstermann et al., 1984; Parantainen et al., 1985) in disorders involving aberrant excitation of neurons, such as epilepsy and migraine, and such disorders often induce sleepiness or sleep (Sand, 1991; Donnet and Bartolomei, 1997; Kotagal, 2001; Foldvary, 2002). These reports also support our finding that SD-induced neuronal COX-2 is involved in NREM sleep via production of these PGs.

The level of COX-2 mRNA has been reported to rise within 30 min of pathological stimuli, such as seizure discharges (Yamagata et al., 1993; Chen et al., 1995), and COX-2 protein to appear 1 hr after seizure activity, peak at 3–4 hr, and remain elevated for 8 hr (Yamagata et al., 1993). Additionally, the content of PGs in the brain has been reported to increase even more rapidly after seizure, the increase in PGD_2 content being approximately 50-fold within 5 min after seizure (Forstermann et al., 1984). We found that, as reported elsewhere (Yamagata et al., 1993; Breder et al., 1995; Caggiano et al., 1996), constitutive expression of neuronal COX-2 is sporadic in the cerebral cortex, even under physiological conditions (Figs. 3, 6B). Thus, the production of PGs in the early phase (less than 1 hr) likely is due to the constitutive expression of COX-2. In the present study, the amount of NREM sleep was significantly increased also within 1 hr after onset of SD. NREM sleep induction in such an early phase following SD is thought to be due to the constitutive expression of COX-2. Because COX-2 is rapidly inactivated following conversion of arachidonic acid to PGs (Hemler and Lands, 1980), expression of the enzyme would have to be both rapid and continuous for hours to increase the amount of NREM sleep. Such a continuous expression of COX-2 in neurons for several hours was histologically confirmed in other SD-induced animals (data not shown).

COX-2 in the brain is known to be involved in NREM sleep induction following several proinflammatory cytokines treatment. NS-398, a selective COX-2 inhibitor, suppresses NREM sleep and fever induced by centrally injected proinflammatory cytokines, including interleukin (IL)-1β or tumor necrosis factor (TNF)-α (Terao et al., 1998a,b; Yoshida et al., 2003). Studies on localization of COX-2 revealed that COX-2 was expressed in endothelial cells in response to such proinflammatory cytokines centrally administrated and contributed to fever evoking (Matsumura et al., 1998; Cao et al., 2001). These observations suggest that the proinflammatory cytokine-induced NREM sleep is due to endothelial COX-2 expression in the brain. In the present study, we induced dramatic expression of COX-2 only in the cortical neurons and obtained evidence that neuronal COX-2 is involved in NREM sleep induction in response to the aberrant neural excitation in the cerebral cortex. In conclusion, we provide here a new line of evidence that neuronal COX-2 is dramatically increased in the cerebral hemisphere following cortical SD and is engaged in signal regulation of NREM sleep induction via subsequent production of PGs.

REFERENCES

Back T, Kohno K, Hossmann KA. 1994. Cortical negative DC deflections following middle cerebral artery occlusion and KCl-induced spreading depression: effect on blood flow, tissue oxygenation, and electroencephalogram. J Cereb Blood Flow Metab 14:12–19.

Beuckmann CT, Lazarus M, Gerashchenko D, Mizoguchi A, Nomura S, Mohri I, Uesugi A, Kaneko T, Mizuno N, Hayaishi O, Urade Y. 2000. Cellular localization of lipocalin-type prostaglandin D synthase (beta-trace) in the central nervous system of the adult rat. J Comp Neurol 428:62–78.

Breder CD, Dewitt D, Kraig RP. 1995. Characterization of inducible cyclooxygenase in rat brain. J Comp Neurol 355:296–315.

Caggiano AO, Breder CD, Kraig RP. 1996. Long-term elevation of cyclooxygenase-2, but not lipoxygenase, in regions synaptically distant from spreading depression. J Comp Neurol 376:447–462.

Cao C, Matsumura K, Shirakawa N, Maeda M, Jikihara I, Kobayashi S, Watanabe Y. 2001. Pyrogenic cytokines injected into the rat cerebral ventricle induce cyclooxygenase-2 in brain endothelial cells and also up-regulate their receptors. Eur J Neurosci 13:1781–1790.

Chen J, Marsh T, Zhang JS, Graham SH. 1995. Expression of cyclooxygenase 2 in rat brain following kainate treatment. Neuroreport 6:245–248.

Cui Y, Kataoka Y, Li QH, Yokoyama C, Yamagata A, Mochizuki-Oda N, Watanabe J, Yamada H, Watanabe Y. 2003. Targeted tissue oxidation in the cerebral cortex induces local prolonged depolarization and cortical spreading depression in the rat brain. Biochem Biophys Res Commun 300:631–636.

Donnet A, Bartolomei F. 1997. Migraine with visual aura and photosensitive epileptic seizures. Epilepsia 38:1032–1034.

Fabricius M, Akgoren N, Lauritzen M. 1995. Arginine-nitric oxide pathway and cerebrovascular regulation in cortical spreading depression. Am J Physiol 269:H23–H29.

Foldvary N. 2002. Sleep and epilepsy. Curr Treat Options Neurol 4: 129–135.

Forstermann U, Seregi A, Hertting G. 1984. Anticonvulsive effects of endogenous prostaglandins formed in brain of spontaneously convulsing gerbils. Prostaglandins 27:913–923.

Gerashchenko D, Okano Y, Urade Y, Inoue S, Hayaishi O. 2000. Strong rebound of wakefulness follows prostaglandin D2- or adenosine A2a receptor agonist-induced sleep. J Sleep Res 9:81–87.

Gold L, Back T, Arnold G, Dreier J, Einhaupl KM, Reuter U, Dirnagl U. 1998. Cortical spreading depression-associated hyperemia in rats: involvement of serotonin. Brain Res 783:188–193.

Gorji A. 2001. Spreading depression: a review of the clinical relevance. Brain Res Brain Res Rev 38:33–60.

Hansen AJ, Zeuthen T. 1981. Extracellular ion concentrations during spreading depression and ischemia in the rat brain cortex. Acta Physiol Scand 113:437–445.

Hayaishi O. 1988. Sleep-wake regulation by prostaglandins D2 and E2. J Biol Chem 263:14593–14596.

Hayaishi O, Urade Y. 2002. Prostaglandin D2 in sleep-wake regulation: recent progress and perspectives. Neuroscientist 8:12–15.

Hemler ME, Lands WE. 1980. Evidence for a peroxide-initiated free radical mechanism of prostaglandin biosynthesis. J Biol Chem 255:6253–6261.

Huang ZL, Qu WM, Li WD, Mochizuki T, Eguchi N, Watanabe T, Urade Y, Hayaishi O. 2001. Arousal effect of orexin A depends on activation of the histaminergic system. Proc Natl Acad Sci U S A 98:9965–9970.

Kataoka Y, Morii H, Imamura K, Cui Y, Kobayashi M, Watanabe Y. 2000. Control of neurotransmission, behaviour and development, by photodynamic manipulation of tissue redox state of brain targets. Eur J Neurosci 12:4417–4423.

Kimura H, Okamoto K, Sakai Y. 1985. Modulatory effects of prostaglandin D2, E2 and F2 alpha on the postsynaptic actions of inhibitory and excitatory amino acids in cerebellar Purkinje cell dendrites in vitro. Brain Res 330:235–244.

Koistinaho J, Chan PH. 2000. Spreading depression-induced cyclooxygenase-2 expression in the cortex. Neurochem Res 25:645–651.

Kotagal P. 2001. The relationship between sleep and epilepsy. Semin Pediatr Neurol 8:241–250.

Lauritzen M, Jorgensen MB, Diemer NH, Gjedde A, Hansen AJ. 1982. Persistent oligemia of rat cerebral cortex in the wake of spreading depression. Ann Neurol 12:469–474.

Leao AAP. 1944. Spreading depression of activity in the cerebral cortex. J Neurophysiol 7:359–390.

Matsumura H, Nakajima T, Osaka T, Satoh S, Kawase K, Kubo E, Kantha SS, Kasahara K, Hayaishi O. 1994. Prostaglandin D2-sensitive, sleep-promoting zone defined in the ventral surface of the rostral basal forebrain. Proc Natl Acad Sci U S A 91:11998–12002.

Matsumura K, Cao C, Ozaki M, Morii H, Nakadate K, Watanabe Y. 1998. Brain endothelial cells express cyclooxygenase-2 during lipopolysaccharide-induced fever: light and electron microscopic immunocytochemical studies. J Neurosci 18:6279–6289.

Miettinen S, Fusco FR, Yrjanheikki J, Keinanen R, Hirvonen T, Roivainen R, Narhi M, Hokfelt T, Koistinaho J. 1997. Spreading depression and focal brain ischemia induce cyclooxygenase-2 in cortical neurons through N-methyl-D-aspartic acid-receptors and phospholipase A2. Proc Natl Acad Sci U S A 94:6500–6505.

Nagata A, Suzuki Y, Igarashi M, Eguchi N, Toh H, Urade Y, Hayaishi O. 1991. Human brain prostaglandin D synthase has been evolutionarily differentiated from lipophilic-ligand carrier proteins. Proc Natl Acad Sci U S A 88:4020–4024.

Nedergaard M, Hansen AJ. 1988. Spreading depression is not associated with neuronal injury in the normal brain. Brain Res 449:395–398.

Nogawa S, Zhang F, Ross ME, Iadecola C. 1997. Cyclo-oxygenase-2 gene expression in neurons contributes to ischemic brain damage. J Neurosci 17:2746–2755.

Ojeda SR, Negro-Vilar A, McCann SM. 1982. Evidence for involvement of alpha-adrenergic receptors in norepinephrine-induced prostaglandin E2 and luteinizing hormone-releasing hormone release from the median eminence. Endocrinology 110:409–412.

Pandey HP, Ram A, Matsumura H, Hayaishi O. 1995. Concentration of prostaglandin D2 in cerebrospinal fluid exhibits a circadian alteration in conscious rats. Biochem Mol Biol Int 37:431–437.

Parantainen J, Vapaatalo H, Hokkanen E. 1985. Relevance of prostaglandins in migraine. Cephalalgia 5(Suppl 2):93–97.

Ram A, Pandey HP, Matsumura H, Kasahara-Orita K, Nakajima T, Takahata R, Satoh S, Terao A, Hayaishi O. 1997. CSF levels of prostaglandins, especially the level of prostaglandin D2, are correlated with increasing propensity toward sleep in rats. Brain Res 751:81–89.

Sand T. 1991. EEG in migraine: a review of the literature. Funct Neurol 6:7–22.

Schwab JM, Schluesener HJ. 2003. Cyclooxygenases and central nervous system inflammation: conceptual neglect of cyclooxygenase 1. Arch Neurol 60:630–632.

Shimizu K, Veltkamp R, Busija DW. 2000. Characteristics of induced spreading depression after transient focal ischemia in the rat. Brain Res 861:316–324.

Shinohara M, Dollinger B, Brown G, Rapoport S, Sokoloff L. 1979. Cerebral glucose utilization: local changes during and after recovery from spreading cortical depression. Science 203:188–190.

Strauss KI, Barbe MF, Marshall RM, Raghupathi R, Mehta S, Narayan RK. 2000. Prolonged cyclooxygenase-2 induction in neurons and glia following traumatic brain injury in the rat. J Neurotrauma 17:695–711.

Terao A, Matsumura H, Saito M. 1998a. Interleukin-1 induces slow-wave sleep at the prostaglandin D2-sensitive sleep-promoting zone in the rat brain. J Neurosci 18:6599–6607.

Terao A, Matsumura H, Yoneda H, Saito M. 1998b. Enhancement of slow-wave sleep by tumor necrosis factor-alpha is mediated by cyclooxygenase-2 in rats. Neuroreport 9:3791–3796.

Tobler I, Deboer T, Fischer M. 1997. Sleep and sleep regulation in normal and prion protein-deficient mice. J Neurosci 17:1869–1879.

Ueno R, Narumiya S, Ogorochi T, Nakayama T, Ishikawa Y, Hayaishi O. 1982. Role of prostaglandin D2 in the hypothermia of rats caused by bacterial lipopolysaccharide. Proc Natl Acad Sci U S A 79:6093–6097.

Yamagata K, Andreasson KI, Kaufmann WE, Barnes CA, Worley PF. 1993. Expression of a mitogen-inducible cyclooxygenase in brain neurons: regulation by synaptic activity and glucocorticoids. Neuron 11:371–386.

Yermakova A, O'Banion MK. 2000. Cyclooxygenases in the central nervous system: implications for treatment of neurological disorders. Curr Pharm Des 6:1755–1776.

Yoshida H, Kubota T, Krueger JM. 2003. A cyclooxygenase-2 inhibitor attenuates spontaneous and TNF-alpha-induced non-rapid eye movement sleep in rabbits. Am J Physiol Regul Integr Comp Physiol 285:R99–R109 [E-pub 2003 Mar].

Radiochim. Acta 97, 83–89 (2009) / DOI 10.1524/ract.2009.1577

Adsorption of Db and its homologues Nb and Ta, and the pseudo-homologue Pa on anion-exchange resin in HF solution

By K. Tsukada[1,*], H. Haba[2], M. Asai[1], A. Toyoshima[1], K. Akiyama[3], Y. Kasamatsu[1], I. Nishinaka[1], S. Ichikawa[1], K. Yasuda[1], Y. Miyamoto[1], K. Hashimoto[1], Y. Nagame[1], S. Goto[4], H. Kudo[4], W. Sato[5], A. Shinohara[5], Y. Oura[3], K. Sueki[6], H. Kikunaga[5], N. Kinoshita[7], A. Yokoyama[8], M. Schädel[9], W. Brüchle[9] and J. V. Kratz[10]

[1] Advanced Science Research Center, Japan Atomic Energy Agency (JAEA), Tokai, Ibaraki 319-1195, Japan
[2] Nishina Center for Accelerator Based Science, RIKEN, Wako, Saitama 351-0198, Japan
[3] Department of Chemistry, Tokyo Metropolitan University, Hachioji, Tokyo 192-0397, Japan
[4] Department of Chemistry, Niigata University, Niigata, Niigata 950-2181, Japan
[5] Department of Chemistry, Osaka University, Toyonaka, Osaka 560-0043, Japan
[6] Department of Chemistry, University of Tsukuba, Tsukuba, Ibaraki 305-8571, Japan
[7] High Energy Accelerator Research Organization (KEK), Tsukuba, Ibaraki 305-0801, Japan
[8] Department of Chemistry, Kanazawa University, Kanazawa, Ishikawa 920-1192, Japan
[9] Gesellschaft für Schwerionenforschung, 64291 Darmstadt, Germany
[10] Institut für Kernchemie, Universität Mainz, 55099 Mainz, Germany

(Received June 10, 2008; accepted in revised form August 4, 2008)

Dubnium (Db) */ Anion-exchange chromatography / Hydrofluoric acid / Fluoride complexation / Atom-at-a-time chemistry*

Summary. Anion-exchange chromatography of element 105, dubnium (Db), produced in the ^{248}Cm(^{19}F, 5*n*)^{262}Db reaction is investigated together with the homologues Nb and Ta, and the pseudo-homologue Pa in 13.9 M hydrofluoric acid (HF) solution. The distribution coefficient (K_d) of Db on an anion-exchange resin is successfully determined by running cycles of 1702 chromatographic column separations. The result clearly indicates that the adsorption of Db on the resin is significantly different from that of the homologues and that the adsorption of anionic fluoro complexes of these elements decreases in the sequence of Ta ≈ Nb > Db ≥ Pa.

1. Introduction

Studies on chemical properties of the transactinide elements with atomic numbers $Z \geq 104$ are extremely interesting and challenging subjects in the fields of modern nuclear and radiochemistry; chemical characterization of these elements explores the new frontiers of the elements in the 7th period of the Periodic Table. From sophisticated experimental investigations so far performed, one can justify placing the elements rutherfordium (Rf) through hassium (Hs) into groups 4 to 8 of the Periodic Table [1–5]. The most recent study on element 112 also suggests this element shows the behavior typical of the group-12 elements [6]. However, some of these experiments show conflicting results and some others are criticized due to unsatisfactory experimental conditions because of the strict restricted experimental conditions on an atom-at-a-time basis [2]. Therefore, it is of great importance to obtain accurate results with good statistics to characterize chemical properties of those elements.

Several attempts to clarify chemical properties of Db in aqueous solution have been made by extraction and ion-exchange chromatography methods [7–13]. Comparative studies of Db with its lighter homologues Nb and Ta, and the pseudo-homologue Pa were carried out. Typical results on the halide complex formation of Db demonstrate that its reversed-phase extraction behavior into aliphatic amines follows closely that of the homologue Nb; it differs considerably from both Pa and Ta in HCl, while it differs mostly from the behavior of Pa in HF [12]. For the distribution coefficient (K_d) of Db in 4 M HF [12], however, only a lower limit was measured, so that a clear distinction in fluoride complexation among those elements has not been established. In our previous works [14–19], the fluoride complexation of Rf belonging to the group-4 elements was investigated through anion- and cation-exchange chromatography together with the lighter homologues Zr and Hf, and the pseudo-homologue Th in HF and in HF/HNO_3 mixed solutions. Those results revealed that the ion-exchange behavior of Rf is remarkably different from that of the homologues, and that the fluoride complexation of Rf is much weaker than that of Zr and Hf, but it is stronger than the complexation of Th.

The present study aims at experimentally determining the K_d of Db on anion-exchange resin in HF and to compare the adsorption of Db with that of the homologues. To find suitable experimental conditions for Db, we first measured K_d values of Nb, Ta, and Pa on anion-exchange resin in 0.97–26.4 M HF through batch experiments using the long-lived radiotracers ^{92m}Nb, ^{177}Ta, and ^{233}Pa. Then, the on-line anion-exchange behavior of ^{262}Db, ^{170}Ta, ^{178m}Ta, and ^{90}Nb was investigated by column chromatographic methods with the Automated Ion-exchange separation apparatus coupled with the Detection system for Alpha spectroscopy,

*Author for correspondence (E-mail: tsukada.kazuaki@jaea.go.jp).

AIDA [16, 20]. The K_d value of Db was successfully determined in 13.9 M HF where the adsorption strength of the anionic fluoro complex of Db is comparable to those of Nb, Ta, and Pa.

2. Experimental

2.1 Batch experiments

The radiotracers ^{92m}Nb ($T_{1/2} = 10.15$ d) and ^{177}Ta ($T_{1/2} = 56.56$ h) were produced *via* the ^{92}Zr(p, n) and ^{177}Hf(p, n) reactions, respectively, by bombarding ^{nat}Zr (65.1 mg cm^{-2}) and ^{nat}Hf (141 mg cm^{-2}) metallic foils at the JAEA tandem accelerator and the RIKEN K70 AVF Cyclotron (nat: natural isotopic abundance). The target materials were dissolved in concentrated HF and the solution was evaporated to dryness. Then, the residue was dissolved in 1.0 M HF and was fed onto an anion-exchange column (Dowex 1 × 8, 200–400 mesh, 7 mm i.d. × 10 mm). The ^{92m}Nb tracer was eluted with 5.0 M HNO_3 and 0.2 M HF mixed solution, while ^{177}Ta was eluted with 26.4 M HF. Protactinium-233 ($T_{1/2} = 27.0$ d) was prepared as an α-decay product of ^{237}Np; ^{233}Pa was separated from ^{237}Np on an anion-exchange column with 9.0 M HCl and 0.025 M HF mixed solution. These radiotracers were stored in polypropylene vessels in 1.0 M HF solution.

For the batch-wise experiments, the anion-exchange resin used was MCI GEL CA08Y, supplied by Mitsubishi Chemical Corporation, a strongly basic quaternary-amine polymer with a particle size of 22 ± 2 μm. The commercially available CA08Y in the chloride form was converted to the fluoride one by washing the column with concentrated HF. Then, the resin was washed thoroughly by the batch method with H_2O and was dried up to a constant weight at 80 °C in a vacuum oven. A portion of 10–15 mg of the resin and 3 mL of the 0.96–26.4 M HF solution containing 50 μL of the tracer solution were added into a polypropylene tube and were shaken for 60 min at 20 °C. After centrifugation, 1.0 mL of the aqueous phase was precisely pipetted into a polyethylene tube and subjected to γ-ray spectrometry using a Ge detector. As a reference sample, 50 μL of the tracer solution was diluted to 1.0 mL with 0.1 M HF in another polyethylene tube. Control experiments without the CA08Y resin were also carried out to evaluate adsorption of the tracers on the inner wall of the polypropylene tube. The number of ^{92m}Nb, ^{177}Ta, and ^{233}Pa atoms used for each batch experiment was 10^{10}–10^{11}. The concentration of HF was determined by titration with a standardized NaOH solution. The details of the preparation of the radiotracers and of the batch-wise experiments are described in a separate paper [21].

2.2 On-line chromatographic experiments with Nb, Ta, and Zr

To investigate the column chromatographic behavior of Nb and Ta on anion-exchange resin, ^{90}Nb ($T_{1/2} = 14.6$ h) and ^{178m}Ta ($T_{1/2} = 9.31$ min) were simultaneously produced *via* the ^{nat}Zr(p, n) and ^{nat}Hf(p, n) reactions, respectively. Each target of about 100 μg cm^{-2} thickness and 7 mm diameter was electrodeposited on a 5.4 mg cm^{-2} aluminum backing. A stack of target foils, three for each ^{nat}Zr and ^{nat}Hf set in a multiple-target chamber, was irradiated with an 11.3-MeV proton beam with an intensity of 2 μA delivered from the JAEA tandem accelerator. The beam passed through two 4.2 mg cm^{-2} HAVAR vacuum windows and 0.2 mg cm^{-2} of helium cooling gas before entering the target chamber. Reaction products recoiling out of the targets were stopped in helium gas (90 kPa), attached to KCl aerosols generated by sublimation of KCl powder at 640 °C and were continuously transported through a Teflon capillary (2.0 mm i.d. × 28 m long) by a He/KCl gas-jet system to the chemistry laboratory. The same experiment using the nuclide ^{89m}Zr ($T_{1/2} = 4.16$ min) produced in the ^{89}Y(p, n) reaction was also conducted to monitor the chromatographic behavior of the group-4 element Zr under identical conditions. To this end, an ^{89}Y metallic foil (112 mg cm^{-2}) was bombarded by the proton beam from the JAEA tandem accelerator.

On-line anion-exchange chromatography was performed using AIDA which consists of a modified ARCA [22] and an automated on-line α-particle detection system [16, 20]. The reaction products transported by the He/KCl gas-jet system were deposited on the collection site of AIDA. After deposition for 180 s, the reaction products were dissolved in 8.0–26.1 M HF and were loaded onto 1.0 mm i.d. × 3.5 mm chromatographic columns filled with the MCI GEL CA08Y resin at a flow rate of 1.2 mL min^{-1}. The effluent fractions were consecutively collected in 8 polyethylene tubes and were assayed by γ-ray spectrometry with Ge detectors to obtain elution curves for Nb, Ta, and Zr. The number of ^{90}Nb, ^{178m}Ta, and ^{89m}Zr atoms present in the anion-exchange experiments was about 10^6.

2.3 On-line chromatographic experiments with Db and Ta

The isotope ^{262}Db ($T_{1/2} = 34$ s) was produced *via* the ^{248}Cm(^{19}F, 5n) reaction. The ^{248}Cm material (97.5% ^{248}Cm) was purified by cation- and anion-exchange separation methods to remove impurities. The ^{248}Cm target of 600 μg cm^{-2} thickness and 5 mm diameter was prepared by electrodeposition of $Cm(NO_3)_3$ in 2-propanol onto a 2.1 mg cm^{-2} beryllium backing foil. To compare the behavior of Db with that of the homologue Ta, the chemical experiment of Db was conducted together with Ta. Therefore, Gd (39.3%-enriched ^{152}Gd of 36 μg cm^{-2} thickness) was admixed in the ^{248}Cm target to simultaneously produce ^{170}Ta ($T_{1/2} = 6.76$ min). The 119.2-MeV ^{19}F beam with an intensity of approximately 280 particle nA delivered from the JAEA tandem accelerator passed through a HAVAR vacuum window (1.8 mg cm^{-2}), helium cooling gas (0.09 mg cm^{-2}), the beryllium target backing, and finally entered the target material at the energy range of 102.1–103.6 MeV. At this incident energy, the excitation function for the ^{248}Cm(^{19}F, 5n)^{262}Db reaction exhibits a maximum cross section of 1.5 ± 0.4 nb [23]. This results in an expected production rate of about 0.4 atoms per minute under the present conditions. The transport efficiency of the gas-jet system was estimated to be 30–35% [23].

On-line anion-exchange chromatography was performed using AIDA. The reaction products transported by the He/KCl gas-jet system were deposited on the collection site of AIDA for 75 s. Then, the products were dissolved in